19

MULTI-PORT TECHNOLOGY AND APPLICATIONS

Moldovan Emilia[1], Bosisio G. Renato[2], Wu Ke[2] and Tatu Serioja O.[1]
[1]*Institut National de la Recherche Scientifique INRS-EMT Montreal*
[2]*Ecole Polytechnique de Montreal*
Canada

1. Introduction

This chapter is dedicated to the description of emerging multi-port circuit designs based on various technologies and their related applications in wireless communication systems and radar sensors.

The multi-port circuit theory was first developed in the 1970s by Engen and other scientists, for accurate automated measurements of the complex reflection coefficient in microwave network analysis. These multi-port pioneers highlighted its usefulness in micro-wave low-cost circuit characterizations (S-parameters). The multi-port techniques were further proposed and developed by Professor R. G. Bosisio and collaborators, for use as a microwave and millimeter wave demodulator in connection with homodyne and heterodyne receivers since 1994. Several multi-port architectures for specific applications have been developed and demonstrated.

Basically, the multi-port is composed of several couplers interconnected by transmission lines and phase shifters. The multi-port acts as an interferometer; its output signals are linear combinations of phase shifted reference and input unknown signals. By using appropriate power detectors at each output and simple analogue signal processing, this circuit can provide I/Q down-conversion or direct modulation.

The chapter describes and analyzes several multi-port circuit implementations and their advantages versus the conventional approaches. Taking benefit of the advancements in fabrication technologies at microwave and millimeter wave frequencies, bulky waveguide circuits have been integrated into various Substrate Integrated Circuits (SICs), including synthesized metallic and dielectric waveguides. For example, Substrate Integrated Waveguides (SIW) consist of a new design scheme based on the concept that a standard metallic rectangular waveguide can be synthesized by two linear arrays of metalized via holes or slots, which are made on the same planar substrate, along with other planar circuits. Despite its dimensional limitations, the conventional Rectangular Waveguide (RWG) technology is still necessary to connect all these SICs to standard millimeter-wave equipment and circuits. Various multi-port circuit schemes and practical realizations, including Miniature Hybrid Microwave Integrated Circuit (MHMIC) and Monolithic Microwave Integrated Circuit (MMIC) implementations, are presented.

Multi-port implementations in Ka-band and V-band receivers for Wireless Local Area Networks (WLANs) dedicated to high data-rate communications are discussed. The multi-port interferometer is an innovative approach, due to its intrinsic properties, such as wide bandwidth, reduced local oscillator power required to perform efficient down-conversion, excellent isolation between input RF ports, and very good suppression of harmonic and spurious products. Multi-ports have been successfully used to demodulate various QAM/PSK signals at hundreds of Mb/s data rates.
Furthermore, multi-port W-band automotive Continuous Wave (CW), V-band Frequency Modulated CW (FMCW), and Phase Coded CW (PCCW) radar sensors with their related relative velocity and distance measurement principles are discussed and compared.
Computed Aided Design (CAD) tools, such as Advanced Design Systems (ADS) of Agilent Technologies and High Frequency Structure Simulator (HFSS) of Ansoft have been used for circuit designs and system simulations. Test bench prototype photographs, and comparative analysis between simulation and measurement results enforce the presentation.

2. The Multi-port Reflectometer

The multi-port, actually a "six-port" circuit, was first developed by Cohn and Weinhouse (1964) to evaluate the phase of a microwave signal, and extended by Engen (1972, a.1977) and other scientists, for accurate automated measurements of the complex reflection coefficient in microwave network analysis. Between 1972 and 1994, similar researches were pursuit by other laboratories, including Poly-Grames Research Center of Ecole Polytechnique of Montreal.
The proposed six-port is a passive circuit, composed of hybrid couplers and/or power dividers, connected by transmission lines. It has two inputs, one for the unknown signal and other for the reference one, and four outputs. The output signals represent linear combinations between the input signals. The evaluation of the reflexion coefficient is based on the measurement of output signal power levels, $|b_i|^2$, where i = 1,…, 4, as follows:

$$P_1 = |b_1|^2 = |Aa + Bb|^2 \quad (1)$$
$$P_2 = |b_2|^2 = |Ca + Db|^2 \quad (2)$$
$$P_3 = |b_3|^2 = |Ea + Fb|^2 \quad (3)$$
$$P_4 = |b_4|^2 = |Ga + Hb|^2 \quad (4)$$

The A to H are complex constants based on multi-port calibration, and **a** and **b** are the incident and the reflected wave, respectively, at the measurement point. Taking into account that each output signal linearly depends on the incident wave power $|a|^2$, and choosing the port 4 as reference, the output signal power levels will only depend on **a**. Hence, if H=0,

$$P_4 = |G|^2 |a|^2 \quad (5)$$

and the normalized output powers of ports 1 to 3 are:

$$p_1 = P_1/P_4 = |A|^2 |a|^2 \ |\Gamma - q_1|^2 \quad (6)$$
$$p_2 = P_2/P_4 = |C|^2 |a|^2 \ |\Gamma - q_2|^2 \quad (7)$$
$$p_3 = P_3/P_4 = |E|^2 |a|^2 \ |\Gamma - q_3|^2 \quad (8)$$

where q_1 = - B/A, q_2 = - D/C, q_3 = - F/E, and A to F are known, due to calibration process. Hence, the reflexion coefficient can be easily obtained using the output power readings.
In order to illustrate the previous theoretical considerations, the bloc diagram of a six-port reflectometer based on four hybrid couplers is presented in Fig. 1.

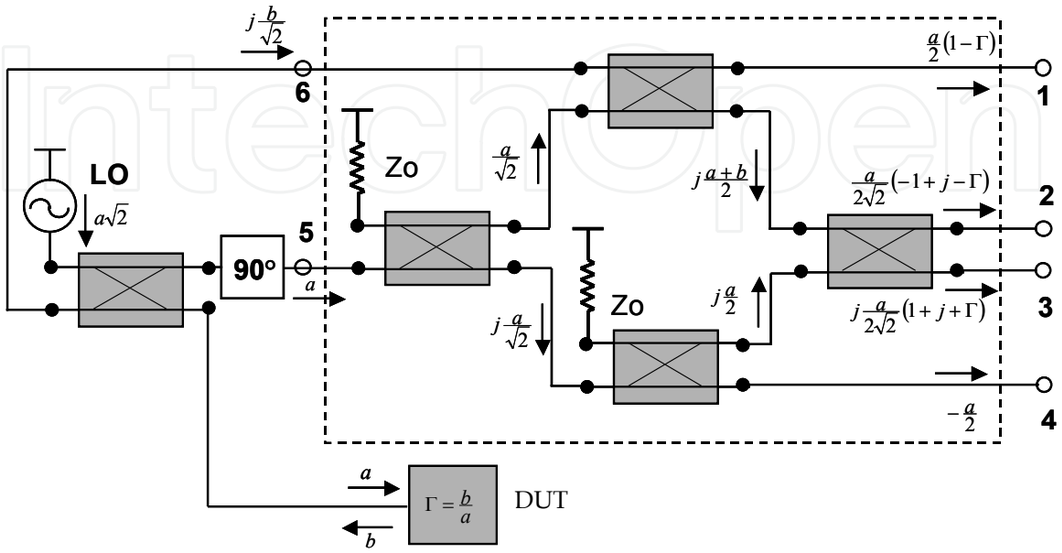

Fig.1. The block diagram of a six-port reflectometer

The reference signal is generated by a local oscillator. Γ = b/a represents the reflection coefficient of the device under test (DUT). The output powers can be expressed as follows:

$$P_1 = (|a|^2/4)\ |\Gamma - 1|^2 \quad (9)$$
$$P_2 = (|a|^2/8)\ |\Gamma - (-1 + j)|^2 \quad (10)$$
$$P_3 = (|a|^2/8)\ |\Gamma - (-1 - j)|^2 \quad (11)$$
$$P_4 = |a|^2/4 \quad (12)$$

By choosing the power of port 4 as reference, due to its non-dependence on Γ, the normalized powers are:

$$p_1 = P_1 / P_4 = |\Gamma - 1|^2 \quad (13)$$
$$p_2 = P_2 / P_4 = ½\ |\Gamma - (-1 + j)|^2 \quad (14)$$
$$p_3 = P_3 / P_4 = ½\ |\Gamma - (-1 - j)|^2 \quad (15)$$

Hence, three circles in complex plan Γ are obtained:

$$|\Gamma - 1|^2 = \sqrt{p_1} \quad (16)$$
$$|\Gamma - (-1 + j)|^2 = \sqrt{2}p_2 \quad (17)$$
$$|\Gamma - (-1 - j)|^2 = \sqrt{2}p_3 \quad (18)$$

These circles, presented in Fig. 2, are centered at q_1 = 1, q_2 = -1 + j and q_3 = -1 – j.

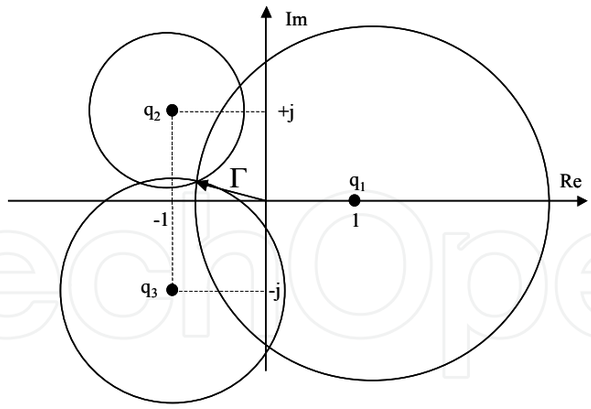

Fig. 2. The family circles in Γ plane

The reflection coefficient Γ is determined by the intersection of these three circles, whose radii are obtained by power measurements. The q_i points depend on the six-port architecture. Ideally, they should be located at the vertices of an equilateral triangle whose center is at the origin. Consequently, $|q_1| = |q_2| = |q_3|$, while the arguments differ by ± 120° (Engen, b. 1977).

3. The Multi-port Interferometer

In the nineties, the idea of a multi-port circuit to be used in direct conversion microwave receivers was proposed for the first time at the PolyGrames Research Center of Ecole Polytechnique de Montreal, Canada, by Professor R.G. Bosisio and his collaborators. The first reported changes were for narrow-band single-carrier demodulation of digital data (Li et al., 1994, 1995, 1996). The multi-port architecture was very similar to the original approach and a calibration process was needed to perform measurements.

The idea of a multi-port interferometer with no need of calibration appeared in 2001 (Tatu et al, 2001). Especially for microwave and millimeter wave frequency, the multi-port successfully replace the conventional I/Q mixers in the receiver front-ends.

3.1 The Multi-port Interferometer Operating Principle

The multi-port circuit presented in Fig. 3, is composed of three 90° hybrid couplers and a Wilkinson power divider. This architecture is typical for a multi-port microstrip implementation. When a standard rectangular waveguide realization is suitable, four 90° hybrid couplers and a 90° phase shifter must be used. The 90° phase shifter will be implemented using a quarter of wave length line, in order to obtain in-phase power split signals, as done by a Wilkinson power divider.

This circuit is designed to perform phase and amplitude measurements without a calibration procedure (Tatu et al, 2005). The phase shift and relative amplitude between RF unknown and reference input signals, $\mathbf{a_6}$ and $\mathbf{a_5}$, respectively, will be obtained by output power measurements.

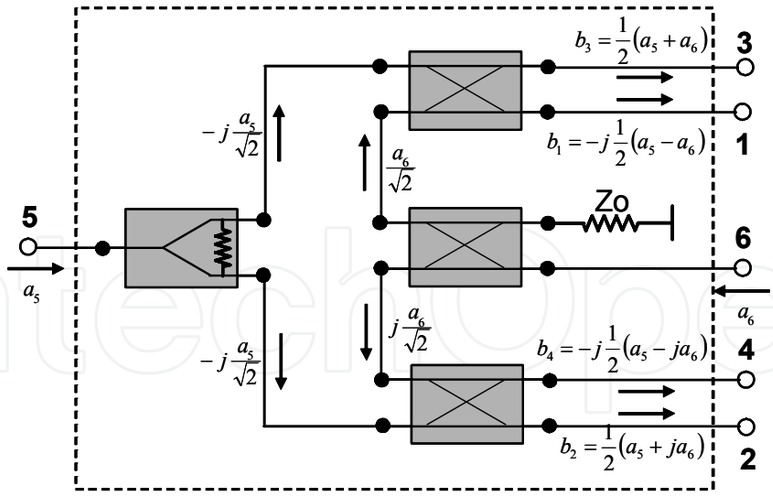

Fig. 3. The multi-port circuit

In a general case, the output signals, b_i, can be expressed in function of the multi-port dispersion parameters (S_{ii}, S_{ij}):

$$b_i = \sum_{j=1}^{6} S_{ij} a_j \text{ , i = 1, …, 6} \tag{19}$$

The scattering matrix of the proposed multi-port phase discriminator can be easily obtained using the diagram of Fig. 3 as follows:

$$\begin{bmatrix} b_1 \\ b_2 \\ b_3 \\ b_4 \\ b_5 \\ b_6 \end{bmatrix} = \frac{1}{2} \begin{bmatrix} 0 & 0 & 0 & 0 & -j & j \\ 0 & 0 & 0 & 0 & 1 & j \\ 0 & 0 & 0 & 0 & 1 & 1 \\ 0 & 0 & 0 & 0 & -j & -1 \\ -j & 1 & 1 & -j & 0 & 0 \\ j & j & 1 & -1 & 0 & 0 \end{bmatrix} \cdot \begin{bmatrix} a_1 \\ a_2 \\ a_3 \\ a_4 \\ a_5 \\ a_6 \end{bmatrix} \tag{20}$$

Supposing a perfect match ($a_1 = a_2 = a_3 = a_4$), the two normalized input waves having α amplitude ratio and $\Delta\varphi = \varphi_6(t) - \varphi_5$ phase difference, can be expressed as follows:

$$a_5 = a \exp(j\, \varphi_5) \tag{21}$$

$$a_6 = \alpha\, a \exp[j\, \varphi_6(t)] = \alpha\, a_5 \exp(j\, \Delta\varphi) \tag{22}$$

Therefore, the four normalized output waves can be expressed in function of input waves and scattering (S) parameters:

$$b_i = a_5 S_{5i} + a_6 S_{6i},\ i = 1, \ldots, 4 \tag{23}$$

More specifically:

$$b_1 = a/2 \exp[j\, (\varphi_5 - \pi/2)]\, \{1 - \alpha \exp[j\, (\Delta\varphi + \pi)]\} \tag{24}$$

$$b_2 = a/2 \exp(j\,\varphi_5)\,\{1 + \alpha \exp[j\,(\Delta\varphi + \pi/2)]\} \quad (25)$$
$$b_3 = a/2 \exp(j\,\varphi_5)\,[1 + \alpha \exp(j\,\Delta\varphi)] \quad (26)$$
$$b_4 = -\,a/2 \exp[j(\,\varphi_5 + \pi/2)]\,\{1 + \alpha \exp[j\,(\Delta\varphi - \pi/2)]\} \quad (27)$$

In order to obtain the DC output signals, four power detectors are connected to the multi-port outputs. As known, the DC output voltage of an ideal power detector is proportional to the square magnitude of the RF input signal:

$$V_i = K_i\,|b_i|^2,\ i = 1, \ldots, 4 \quad (28)$$

Supposing that identical power detectors are used, $K_i = K$, the DC output voltages will be:

$$V_1 = K|b_1|^2 = K\,a^2/4\,[1 + \alpha^2 - 2\alpha\cos(\Delta\varphi)] \quad (29)$$
$$V_2 = K|b_2|^2 = K\,a^2/4\,[1 + \alpha^2 - 2\alpha\sin(\Delta\varphi)] \quad (30)$$
$$V_3 = K|b_3|^2 = K\,a^2/4\,[1 + \alpha^2 + 2\alpha\cos(\Delta\varphi)] \quad (31)$$
$$V_4 = K|b_4|^2 = K\,a^2/4\,[1 + \alpha^2 + 2\alpha\sin(\Delta\varphi)] \quad (32)$$

Each function $V_i(\Delta\varphi)$ is periodical of 2π and the output minimum voltages are shifted by $\pi/2$ one to other. The normalized DC output voltage variations in a 360° input signal phase difference shift are presented in Fig. 4 ($v_i = V_i/K|b_i|^2$, i = 1, …, 4). The input signals are considered of the same amplitude ($\alpha = 1$).

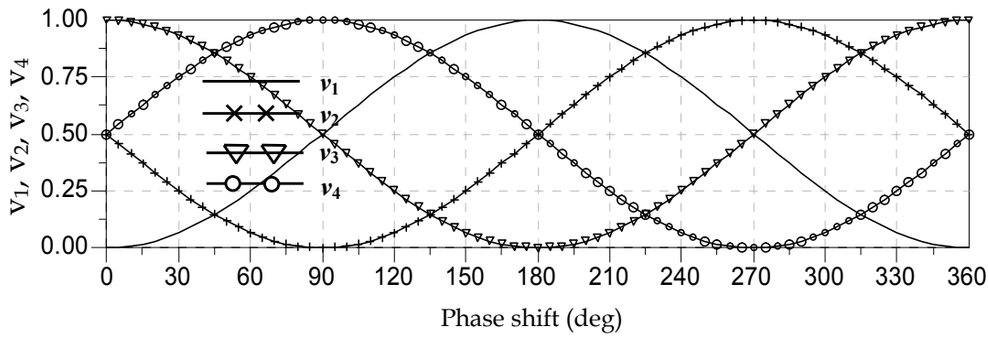

Fig. 4. Normalized DC output voltage variations for a 360° shift of input signal phase difference

As seen, the minimal values are shifted by 90° multiples. In addition, the output voltages at ports 1 and 3, and 2 and 4, respectively, are phase opposites. Therefore, the output quadrature signals I/Q can be obtained using a differential approach.
In the I/Q complex plane, a Γ vector can be defined based on the four output voltages:

$$\Gamma = (V_3 - V_1) + j(V_4 - V_2) \quad (33)$$

and the I/Q signals are:

$$I = V_3 - V_1 = \alpha\,K\,a^2\cos(\Delta\varphi) \quad (34)$$
$$Q = V_4 - V_2 = \alpha\,K\,a^2\sin(\Delta\varphi) \quad (35)$$

Previous equations show that, theoretically, the output signal DC offset is equal to zero. In practice, this value is not null, but can be reduced by a rigorous design of the multi-port circuit and its power detectors.
Based on previous equations, the Γ vector can be expressed as:

$$\Gamma = \alpha K a^2 \exp(j \Delta\varphi) \tag{36}$$

It is to be noted that the Γ magnitude is proportional to the amplitude ratio between the input signals and its phase represents their phase difference:

$$\varphi_\Gamma = \Delta\varphi = \varphi_6 - \varphi_5 \tag{37}$$

This biunique correspondence between RF and baseband domains proves that the multi-port circuit can act as a phase discriminator.
In the same time, it can be demonstrated that this circuit can also act as an amplitude discriminator. If the input signal is PSK modulated, the Γ circle radius is a function of the input multi-port power, as expected. As known, the input RF power is equal to the square magnitude of the normalized input wave. According to equation (36) and the normalized wave definition, the magnitude of Γ became:

$$|\Gamma| = \alpha K |a|^2 = (P_{IN}/P_{REF})^{1/2} K P_{REF} = K (P_{IN} P_{REF})^{1/2} \tag{38}$$

where P_{IN} and P_{REF} represent the powers of the RF input and local oscillator reference signals, respectively. Supposing a variation of RF input signal power from P_{IN1} to P_{IN2}, and assuming a constant local oscillator power, this will be proportional to a variation of Γ magnitude:

$$|\Gamma_1| / |\Gamma_2| = (P_{IN1}/P_{IN2})^{1/2} \tag{39}$$

For a dB quantification of this relation:

$$20 \log(|\Gamma_1| / |\Gamma_2|) = 20 \log[(P_{IN1}/P_{IN2})^{1/2}] = 10 \log (P_{IN1}/P_{IN2}) \tag{40}$$

and

$$|\Delta\Gamma|_{dB} = \Delta P_{IN\ dB} \tag{41}$$

The previous equation shows that the amplitude variation of the baseband signal in complex plane is equal to the RF input signal power variation in the same time range, for a constant reference signal. This property proves the capability of the multi-port circuit to also act as an amplitude discriminator.
Equations (37) and (41) represent the fundament of multi-port theory, proving the potential of this circuit to demodulate various PSK and QAM modulated signals.

3.2 The Multi-port Practical Implementations

The multi-port circuit was implemented in various architectures and technologies. The choice of the fabrication technology depends on the operating frequency and application.

Microstrip Monolithic Microwave Integrated Circuits (MMIC) and Miniature Hybrid Microwave Integrated Circuits (MHMIC) were preferred for prototypes at Ka and V band frequencies, for various communication receivers and radar sensors, in homodyne and heterodyne implementations. The Substrate Integrated Waveguide (SIW) and Standard Rectangular Waveguide (SRW) technologies were used at W band frequencies, to support higher power levels, requested in radar sensors and phase noise measurement applications.

3.2.1 MHMIC and MMIC Microstrip Multi-port Implementations

During the time, various multi-port circuits were designed and fabricated in microstrip technology, for different applications. The typical topology of the circuit was illustrated in Fig. 3. This multi-port circuit is designed as the core of an I/Q demodulator, using three 90° hybrid couplers and a Wilkinson power divider.

The relative power reading of the output signals gives sufficient information to determine the phase shift between the two RF inputs, thereby realizing a QPSK demodulator.

The Momentum of Advanced Design System (ADS) software of Agilent Technology was used for the circuit design in microstrip implementations.

A good design targets the reflection and insertion loss, and the isolation between the RF and reference signal. It is to be mentioned that, due to its architecture, the insertion loss of an ideal multi-port is 6 dB. The isolation of the inputs is a very important criterion of the communication systems. The phase difference between the two input signals is evaluated by linear combinations of four output signals, detected at ports 1, 2, 3 and 4. In order to reduce the DC offset caused by the multiple reflections at the outputs, related return losses at the operating frequency must be excellent.

3.2.1. a. Ka-band Microstrip Implementations

At the beginning, a multi-port circuit was designed at Ka-band frequencies, in MHMIC and MMIC technologies, to be used in a direct conversion receiver for high speed QPSK communications (Tatu et al., 2001).

The circuit was first designed and fabricated in hybrid technology, on a 250 μm ceramic substrate with a relative permittivity ε_r = 9.9. The layout and related photograph of the MHMIC multi-port Ka-band implementation are shown in Fig. 5.

The distributed parameter multi-port, composed of three compact 90° hybrid couplers and a Wilkinson power divider, is placed in the middle of the circuit layout. Surface-mounted RF Schottky diodes and related wide-band matching circuit networks are connected to multi-port outputs. The MHMIC chip outer dimensions are 23 x 23 mm.

At the central operating frequency, the measured reflection coefficients S_{11} to S_{66} are less than -24 dB and the measured isolation between RF and reference ports, S_{56}, is found to be at least -27 dB. The measured transmission coefficients are close to the theoretical predicted value of -6 dB. The detection circuit is designed to cope with a wideband operation (23 to 31 GHz) using HSCH-9161 type zero-bias Schottky diodes.

The MMIC multi-port module is fabricated on a 100 micron TriQuint's GaAs substrate with a relative permittivity ε_r = 12.9 (Tatu et al., 2002).

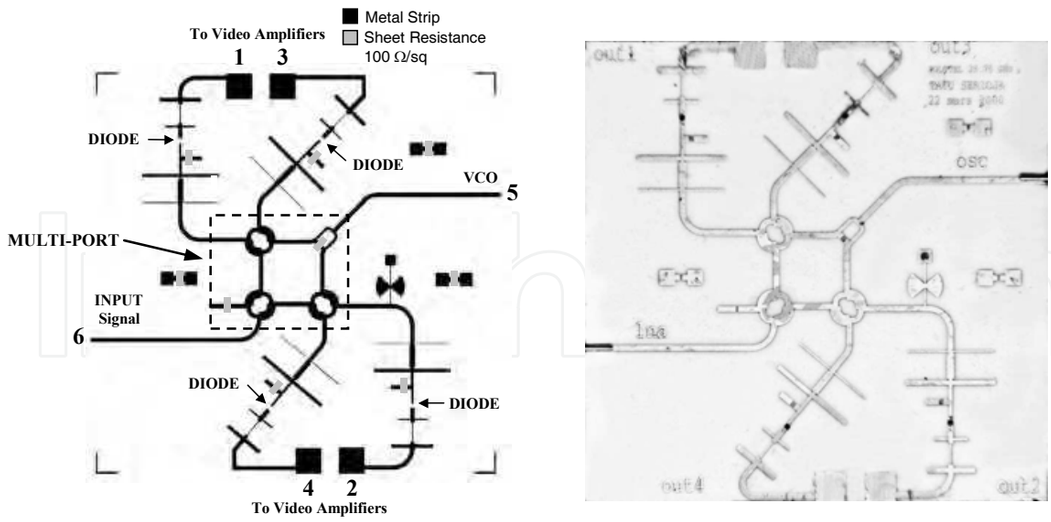

Fig 5. MHMIC Ka-band layout (and photograph) of multi-port circuit with power detectors

Three different implementations of the 90° hybrid coupler in a frequency range of 6 GHz, between 24 and 30 GHz, with distributed parameters, discrete components, and a combination of both methods, are realized and compared. The distributed parameter implementation is large in size (1.39 mm²), but it has excellent S parameter performances. The discrete element coupler has a very small size, but the fabrication process tolerances at this frequency range lead to poor S parameter performances. The hybrid implementation using high impedance transmission lines and capacities leads to very good S parameter performances.

Fig. 6.a shows the RF topology of a wideband millimeter wave MMIC distributed parameter multi-port circuit with integrated RF Schottky diodes (marked by arrows) and related matching networks, using 50 Ω transmission lines. The circuit is realized in a 100 micron GaAs substrate. Its size is about 4 x 4 mm.

In order to reduce the size of the MMIC circuit, a new approach is proposed. The couplers are realized using high impedance transmission lines and discrete components (shunt capacitors of 200 fF, loaded near the ports of the hybrid couplers). The diameter of these couplers is 600 microns, representing 45% of the first implementation, with a diameter of 1330 microns. The same RF Schottky diodes are used in this implementation. Their matching networks are also realized using shunt capacitors and high impedance transmission lines.

Fig. 6.b shows the RF topology of this hybrid circuit. Its size is reduced to 2 x 3 mm, representing about 37% of the first implementation.

In order to characterize the MMIC multi-port circuit, a study of its S parameters in a 6 GHz range around the central frequency, was made. The magnitude and phase of the S parameters versus the operating frequency are close to the predicted values. The results of both implementations (see Figs. 6.a and b) are practically similar.

In the operating band, the magnitudes of the transmission coefficients, illustrated in Figs. 7.a and b, are close to the theoretically predicted values of -6 dB. The phase shifts between the same parameters are multiples of 90° over the considered frequency band (6 GHz), as seen in Figs. 8.a and b.

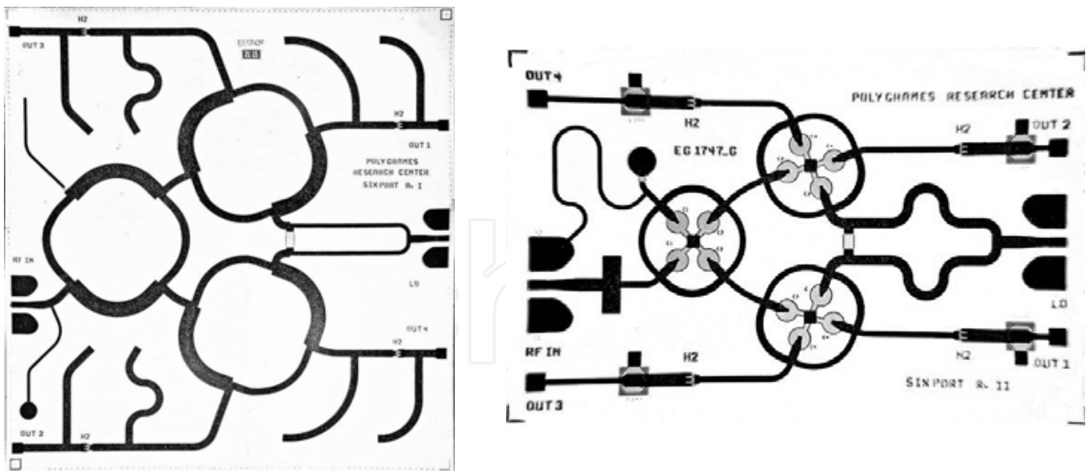

(a) (b)

Fig. 6. MMIC multi-port module: (a) distributed parameters; (b) hybrid implementation

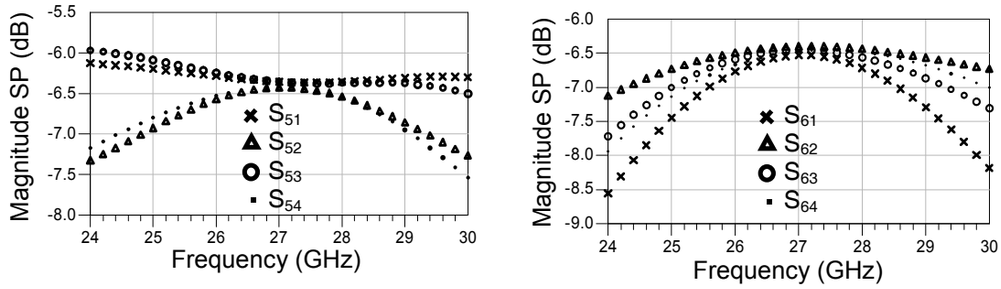

(a) (b)

Fig.7. Magnitude of transmission coefficients vs. the operating frequency: (a) LO; (b) RF

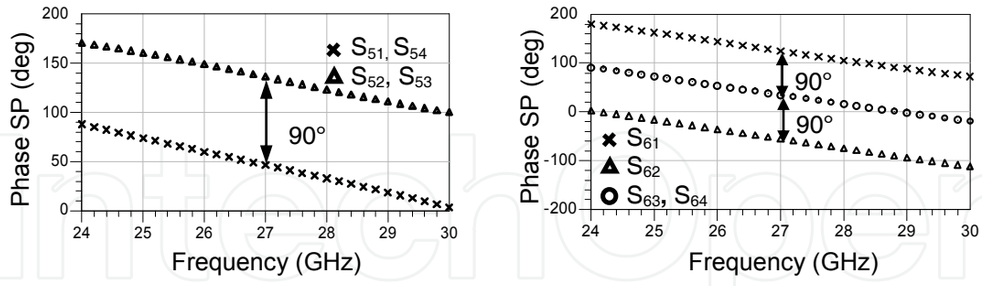

(a) (b)

Fig. 8. Phase of transmission coefficients vs. the operating frequency: (a) LO; (b) RF

Fig. 9 shows excellent return loss and isolation of RF inputs (S_{55}, S_{66}, S_{56}) in the considered frequency band, for the MMIC multi-port module, including the Schottky diodes. Therefore, as for the MHMIC circuit, it can be concluded that the influence of DC offsets in the demodulating process is significantly minimized.

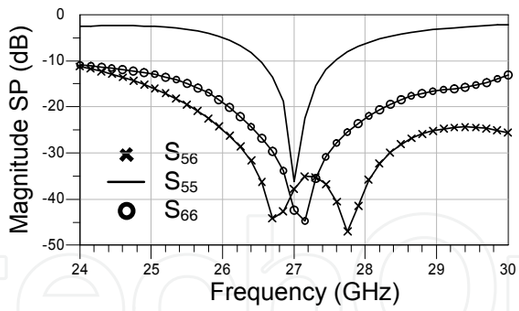

Fig. 9. Return loss and isolation of input ports vs. the operating frequency

Considering a QPSK modulation, the RF design of the multi-port circuit is such that only one of four possible modulation states is correctly identified, at any given time, by an analogue decoder. Harmonic balance simulation of the MMIC multi-port module is shown in Fig. 10. The local oscillator (LO) and RF input power levels were both set at –3 dBm. As seen, each output voltage of the multi-port has a single maximum value over a 360° phase-shift between input signals.

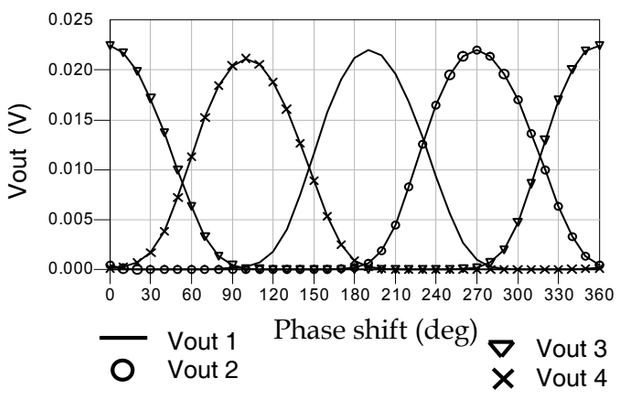

Fig. 10. MMIC multi-port output voltages vs. the phase difference of input signals

3.2.1. b. V-band Microstrip Implementation

A V-band multi-port circuit was designed in MHMIC technology using a 125 μm ceramic substrate, having a relative permittivity of 9.9 (Boukari et al., 2009). The circuit topology is based on four 90° hybrid couplers connected by 50 Ω microstrip transmission lines, as seen in the microphotograph of Fig. 11. In order to avoid reflections at the two unused ports of the multi-port circuit, 50 Ω loads are connected to open circuited quarter-wave transmission lines (representing virtual RF short-circuits). The hybrid coupler connected to LO port (5) together with the 90° phase shifter (implemented using an additional quarter-wave transmission line on curved branch) is equivalent to an in-phase 3 dB power divider.

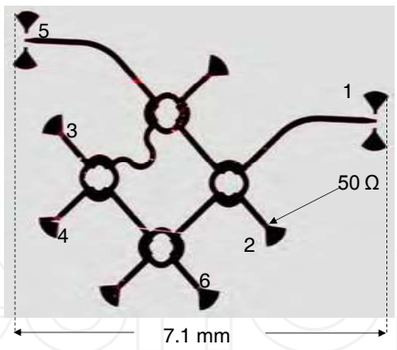

Fig. 11. The microphotograph of the V-band MHMIC multi-port

On-wafer multi-port S parameter measurements are performed using an Agilent PNA millimeter-wave network analyzer, over 4 GHz band, between 60 and 64 GHz. Fig. 12 presents typical S parameter variations for this multi-port circuit.

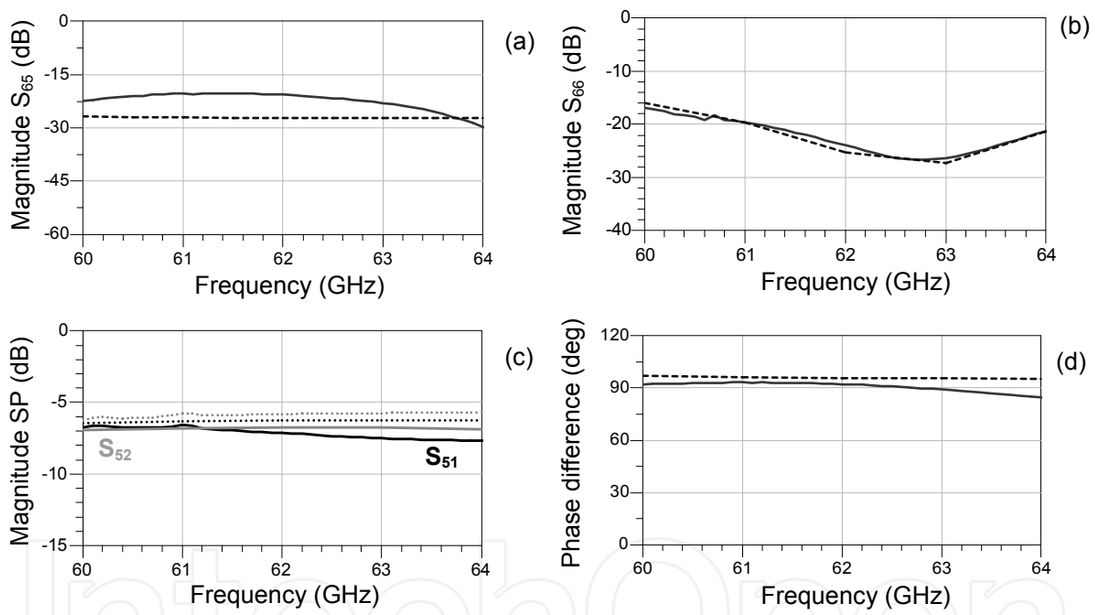

Fig. 12. Simulated (dotted line) and measured (continuous line) S-parameters of the V-band multi-port

As seen, good results are obtained for return loss and isolation between the RF input ports. In addition, power split is quasi-constant over the band and close to the theoretical value of -6 dB. The use of the V-band hybrid couplers determinates a quasi-constant 90° phase difference over a wide band, suitable for a good I/Q mixer.

In order to demonstrate that the multi-port is a four "qi points" circuit having all points spaced by 90º, a harmonic balance simulation is performed at 60 GHz using a multi-port model based on S-parameter measurement results. Power detectors are connected at the four outputs. The phase difference between the millimeter-wave inputs is swept in a 360º range and the RF input signal power is set to 0 dBm.

The multi-port detected output voltages versus the phase difference are shown in Fig. 13. As seen, the output voltage minimum values are shifted by 90° multiples, as requested for this multi-port architecture. In addition, the output voltages at ports 1 and 3, and 2 and 4, respectively, are phase opposites. Therefore, I/Q output signals can be obtained using a differential approach, as illustrated by equations (34) and (35).

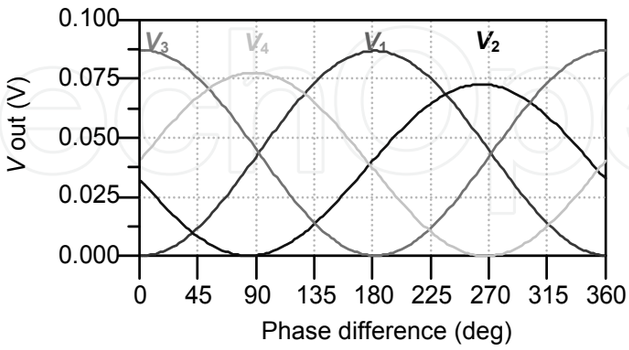

Fig. 13. Multi-port detected voltages vs. input phase difference

Two multi-port implementations were designed and fabricated for automotive radar applications (Boukari et al., 2009). Different topologies are used: three Hybrid and one Wilkinson couplers, and two hybrid and two rat-race couplers, respectively. Their microphotographs are showed in Figs. 14.a and b.

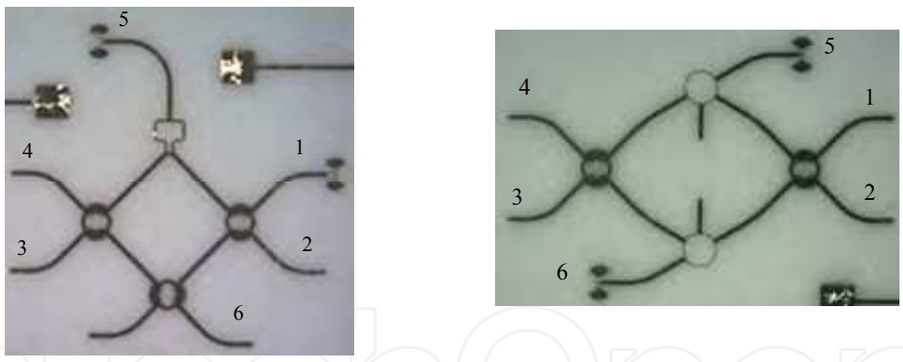

(a) (b)

Fig. 14. Microphotographs of multi-ports implemented using: (a) hybrid and Wilkinson couplers; (b) hybrid and rat-race couplers

On-wafer multi-port S parameter measurements were performed using an Agilent PNA millimeter-wave network analyzer, over 30 GHz band, between 60 and 90 GHz.
Fig. 15 presents some typical S parameters of the multi-port presented in Fig. 14 (a). Both isolation and return loss have very good values at the operating frequency of 77 GHz (Figs. 15.a and b). Fig. 15.c shows the power splitting between the LO port and two adjacent output ports (S_{51} and S_{52}). The error of related phase difference from 90° is minimal at the operating frequency (Fig. 15.d). In addition, Fig. 16 presents the same S parameters for the multi-port presented in Fig. 15 (b). As in the previous case, measures are presented in

continuous line and simulations in dotted line. Similar conclusions can be drawn at the operating frequency and over the whole 30 GHz band.

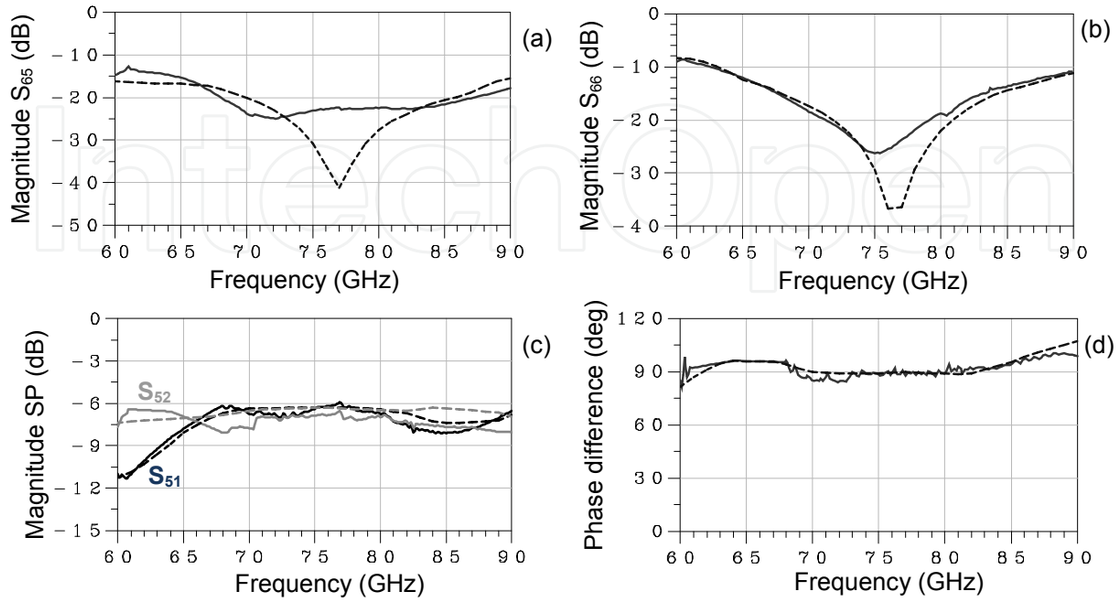

Fig. 15. Simulated (dotted line) and measured (continuous line) S parameters of the multi-port of Fig. 15 a

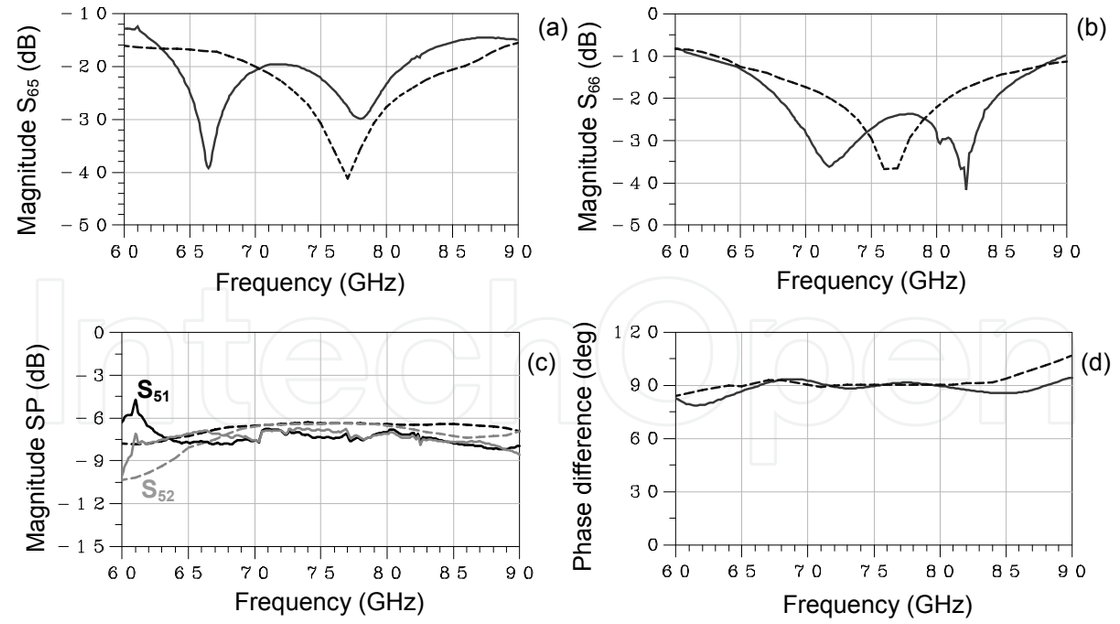

Fig. 16. Simulated (dotted line) and measured (continuous line) S parameters of the multi-port of Fig. 15. b

3.2.2 Rectangular Waveguide Multi-port Implementation

The circuit was designed using the High Frequency Structure Simulator (HFSS) software of Agilent Technologies, and fabricated in a metal block of brass using a computer numerically controlled (CNC) milling machine. The operating frequency was selected at 94 GHz, related to a specific radar sensor application. WR-10 standard rectangular waveguide corresponding to W frequency band was used to generate the circuit and to connect it to the network analyzer, or other front-end components, such as antennas, power and low-noise amplifiers, power detectors, couplers or phase shifters. For this implementation, a four hybrid coupler topology was used. The photographs of the RWG multi-port and related hybrid coupler are presented in Fig. 17.

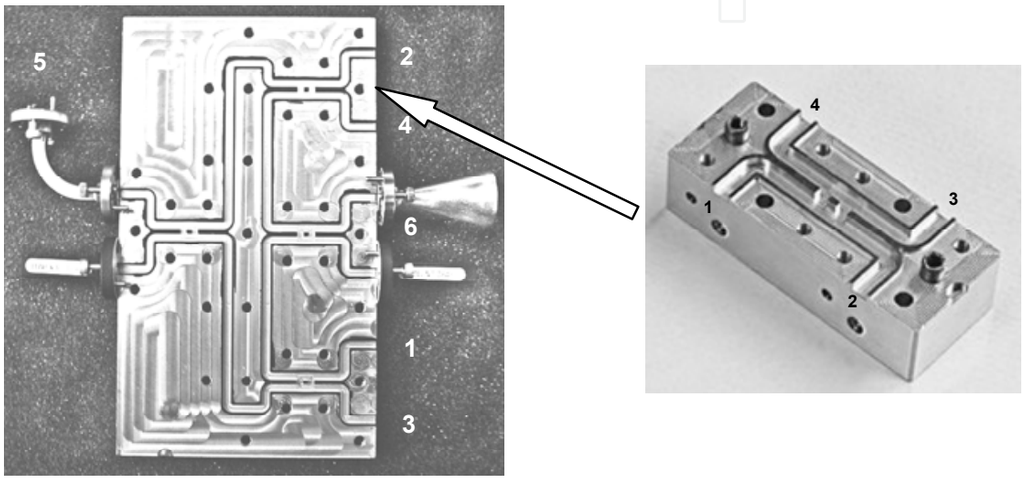

Fig. 17. Photographs of RWG multi-port and related hybrid coupler

An Anritsu 37397C Network Analyzer was used to measure the S-parameters (Moldovan et al, 2004). Due to the geometrical limitations, as seen in the circuit photography, it was impossible to measure all specific S-parameters (e.g. 6-4, 1-3, 2-4) using the standard network analyzer equipment. Fig. 18 shows the measured return losses and the isolation related to the input ports. A maximal isolation of -26 dB is obtained at 94.6 GHz and less than -20 dB were obtained for both RF and LO input return losses, at 95 GHz.

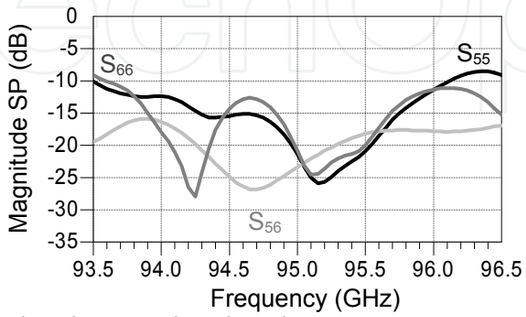

Fig. 18. Return losses and isolation related to the input ports

Output matches and isolation between output ports have also been measured, as seen in Figs. 19.a and b. The return losses are less than -15 dB, over a 1.5 GHz band, between 94.2 and 95.7 GHz. A minimum isolation of -25 dB between output ports 2 and 4 at 94.7 GHz is obtained. Typical measured transmission coefficients are also presented in Figs. 20.a and b. The magnitudes of the measured transmission S-parameters S_{51}, S_{54} and S_{62} are about -7.5 dB between 94.6 and 95 GHz. Therefore, a supplementary insertion loss of 1.5 dB, comparative to the ideal value of -6 dB, is obtained.

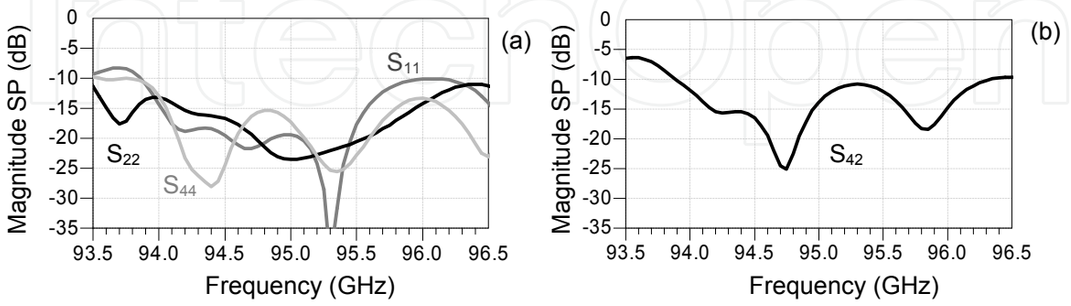

Fig. 19. (a) Return losses at output ports 1, 2 and 4; (b) isolation between outputs 2 and 4

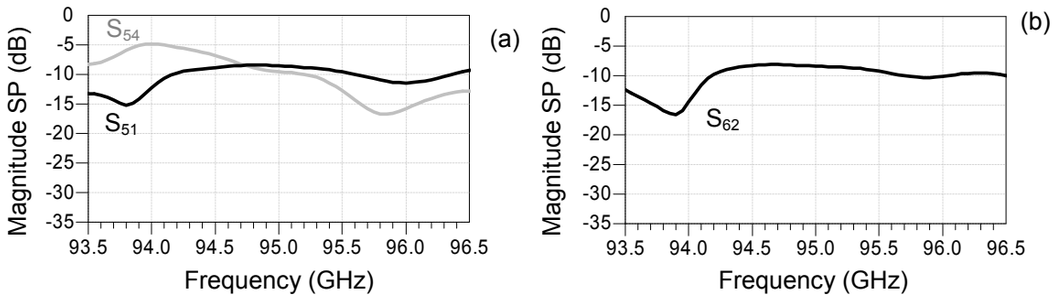

Fig. 20. Transmission coefficients between: (a) LO input and outputs 1 and 4; (b) RF input and output 2

3.2.3 Substrate Integrated Waveguide Multi-port Implementation

The substrate integrated waveguide (SIW) technology, that is part of the substrate integrated circuit family, presents a new design scheme based on the concept that a standard metallic waveguide can be synthesized and fabricated with linear arrays of metalized via holes or posts, which are realized on the same planar substrate along with other planar circuits such as micro-strip and coplanar waveguides.

This dielectric-filled integrated waveguide presents a similarity to its rectangular counterpart even though it has a non-conventional width/height aspect ratio and different guided-wave modal behaviors. The SIW technology allows a high degree of integration of millimeter-wave circuits at low cost, as compared to the standard waveguide technology. The resulting size of circuits can be significantly reduced due to the inherent dielectric effects (Moldovan et al., 2006).

The multi-port circuit, to be used in the RF module of a millimeter wave radar sensor, is designed and fabricated on a low-cost standard 254 μm alumina substrate. Commercial full-wave software (High Frequency Structure Simulator - HFSS version 9.1) of Ansoft

Corporation is used for the design and simulation. To measure the S-parameters in W-band, an Anritsu 37397C Network Analyzer is used.
The multi-port architecture is based on four 90° hybrid couplers. Photographs of the SIW multi-port circuit alone and integrated in the metallic fixture, are presented in Figs. 21. a and b.

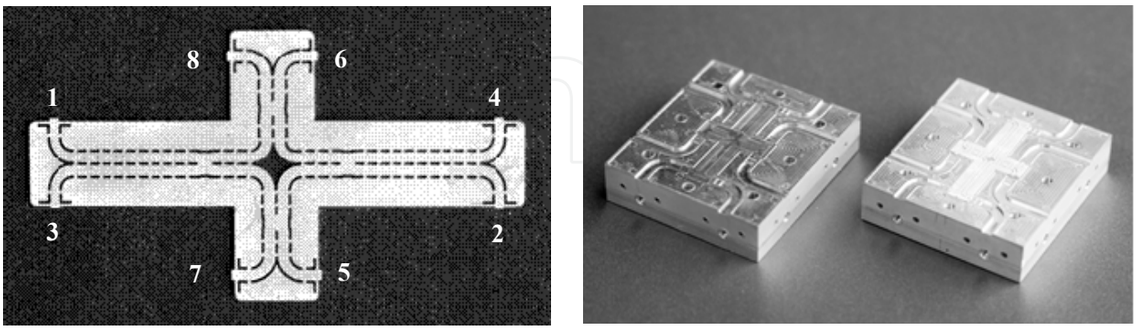

Fig. 21. Photographs of the SIW multi-port circuit

The outer dimensions of the SIW multi-port circuit, of 18.6 by 35.7 mm, are related to WR-10 standard flanges. The circuit is mounted on a metallic fixture, providing SIW to WR-10 transitions, in order to perform S-parameter measurements and to allow the connections to other millimeter wave circuits. The outer dimensions of the fixture, of 43 by 50 mm, are restricted by the physical dimensions of the standard WR-10 flanges, having a diameter of 19 mm. The machined rectangular waveguide part is fabricated in a metal block of brass using a computer numerically controlled milling machine. In order to accommodate the SIW alumina circuit, the metal block provides a central cavity. The alumina substrate is processed using laser micromachining equipment. The slots, the top and the bottom of the circuit are metalized.
The simulations and measurements are performed over a 4 GHz frequency band, between 92 and 96 GHz. In order to improve the sensor performances, the input ports must be isolated from each other as much as possible. The leakage of the reference signal to port 6 must be negligible as compared to the received signal. Fig. 22 shows comparative simulation (continuous line) and measured (dotted line) results of the input isolation over the frequency band. At least 20 dB of isolation is obtained in a wide band, covering the operating frequency of 94 GHz.

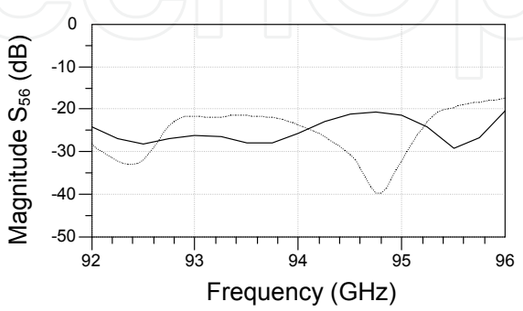

Fig. 22. Simulated and measured (dotted line) isolation between input ports

Using the same convention, comparative simulation and measurement results of return losses related to all output ports are presented in Fig. 23. It can be seen that about 20 dB of the return loss magnitude is obtained at the operating frequency of 94 GHz.

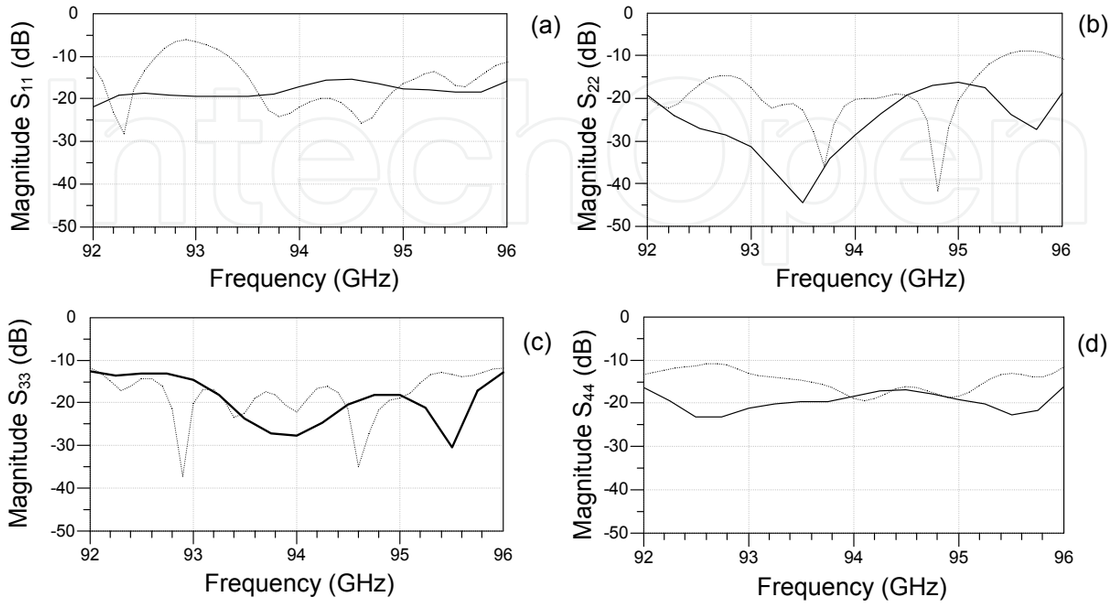

Fig. 23. Simulated (continuous line) and measured (dotted line) output return losses

It is to be noted that, because each RF input signal passes through two hybrid couplers, an ideal multi-port circuit has an equal split of 6 dB of the input signal at the central frequency. Simulation results presented in Fig. 24 are very close to this theoretical value. In the case of the proposed multi-port circuit, equipped with SIW to WR-10 rectangular wave guide transitions to all the ports, an additional loss of around 4 dB must be considered. Therefore, as seen in the figures below, a measured insertion loss of about 10 dB is achieved.

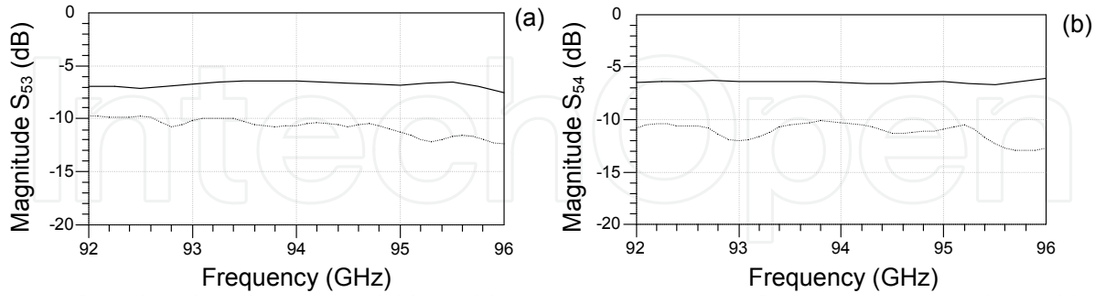

Fig. 24. Simulated and measured (dotted line) transmissions: LO port to outputs: (a) 3; (b) 4

Due to the use of 90° hybrid couplers, the phase difference between the transmission S-parameters must be multiples of 90°. Fig. 25 presents a typical phase measurement of two consecutive transmissions between the reference ports and output ports 3 and 4. As it can be seen in this figure, an equal phase difference of around 90° is obtained in the frequency band.

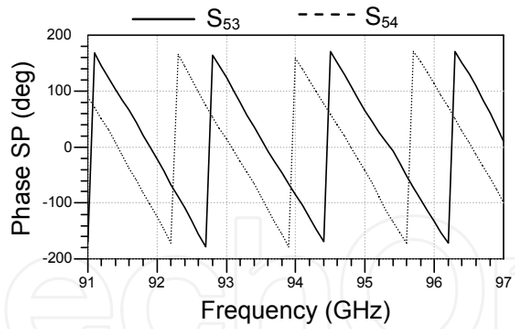

Fig. 25. Measured S parameter phases of consecutive transmission parameters S_{53} and S_{54}

According to equations (29) to (32), the multi-port output waves are linear combinations of the input waves. Measured S-parameters are used to calculate one of these output magnitudes versus the phase shift between the RF input waves. As illustrated in Fig. 26, for each output wave, periodical maximum and minimum values are obtained. The period of the output wave is 360°. In this calculation, the power of each RF input signal was set to 0 dBm. Due to the constructive and destructive interferences, the output signals oscillate between a minimum and a maximum. The minimum value is theoretically zero. However, in practice, due to the constructive errors, this is a non-zero value and it represents a criterion of quality of the multi-port design. As shown by this diagram, the output minimum value is less than 3% of its maximum. So, it can be concluded that very good measurement results are obtained.

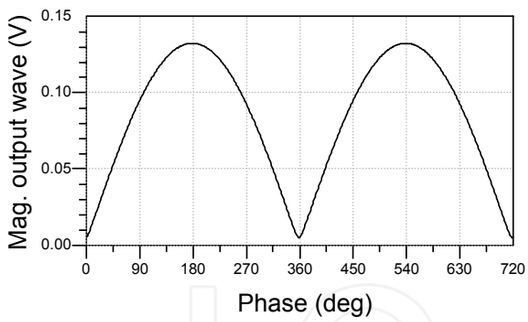

Fig. 26. Calculated output wave variation vs. input signal phase difference

4. The Multi-port Quadrature Demodulator

Similarly as in the analysis of the multi-port interferometer, we assume that there are two normalized input waves, a reference one, a_5, generated by a local oscillator, and a_6, an RF time dependent signal, of different amplitude, phase and even frequency (heterodyne case). Therefore, the output I/Q signals are:

$$i(t) = v_3(t) - v_1(t) = K\,\alpha(t)\,|a|^2\cos[-\Delta\omega t + \Delta\varphi(t)] \quad (42)$$

$$q(t) = v_4(t) - v_2(t) = K\,\alpha(t)\,|a|^2\sin[-\Delta\omega t + \Delta\varphi(t)] \quad (43)$$

Previous equations show that the multi-port circuit, together with four power detectors and two differential amplifiers can successfully replace a conventional I/Q mixer.
In practice, for a multi-port heterodyne receiver, the carrier frequency ω is close to the local oscillator frequency ω_0. Therefore, these are low IF heterodyne receivers. However, if $\omega_0 = \omega$, I/Q conversion is obtained in a homodyne architecture. Hence, $\Delta\omega = 0$ and the quadrature output signals are:

$$i(t) = v_3(t) - v_1(t) = K\,\alpha(t)\,|a|^2\cos[\Delta\varphi(t)] \quad (44)$$

$$q(t) = v_4(t) - v_2(t) = K\,\alpha(t)\,|a|^2\sin[\Delta\varphi(t)] \quad (45)$$

This aspect can be considered as an important advantage of the proposed receivers compared to the conventional ones, because the same multi-port front-end can be used for both heterodyne and homodyne architectures. In addition, signal to noise ratio is improved and the cost of additional hybrid couplers and the two Schottky diodes is compensated by the reduced cost of the IF stage (IF mixers instead of the conventional IF I/Q ones).

4.1 Communication System Applications

In order to validate the previous theoretical results, a test bench using available equipments and a prototype based on Ka-band multi-port of Fig.5, is built.
Fig. 27 shows the block diagram and the photography of this test bench. The PSK/QAM modulated signal and the reference signal of 250 MHz are generated using an HP-8782 vector signal generator. This generator can provide various PSK/QAM modulated signals. The Ka-band modulated signal and the reference signal are obtained using a local oscillator LO (Wiltron frequency synthesizer model 6740B), a Wilkinson power divider (W) and two SU26A21D side-band up-converters. The direct conversion and analog splitting are simultaneously obtained using the Ka-band multi-port demodulator. The demodulated signal constellation can be directly visualized using an oscilloscope.

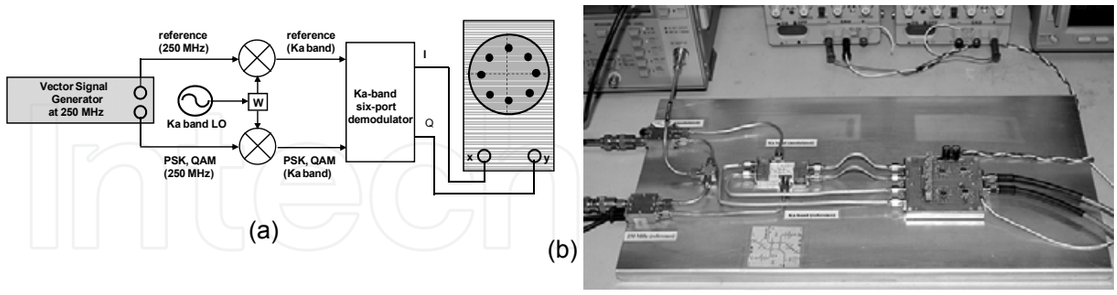

Fig. 27. Block diagram (a) and photograph (b) of the Ka-band demodulator test bench

Fig. 28 shows various demodulated constellations of 40 Mb/s PSK/QAM signals, on oscilloscope screen, using previously described Ka-band prototype (Tatu et al (2005)). As seen, all clusters of demodulated constellations are very well positioned and individualized, validating the multi-port approach.
Fig. 29 (a) shows simulated and measured Bit Error Ratio (BER) in the case of QPSK signals, as a function of E_b/N_o, where E_b is the average energy of a modulated bit and N_o is the noise power spectral density. It can be seen that the BER is less than $1.0E^{-6}$ for E_b/N_o higher than

11 dB over the operating band (23 – 31 GHz). However, outside the upper and lower limits of the operating bandwidth, the BER rises up rapidly, as it is measured to be greater than $1.0E^{-4}$ at 22 GHz and 32 GHz for the same value of E_b/No.

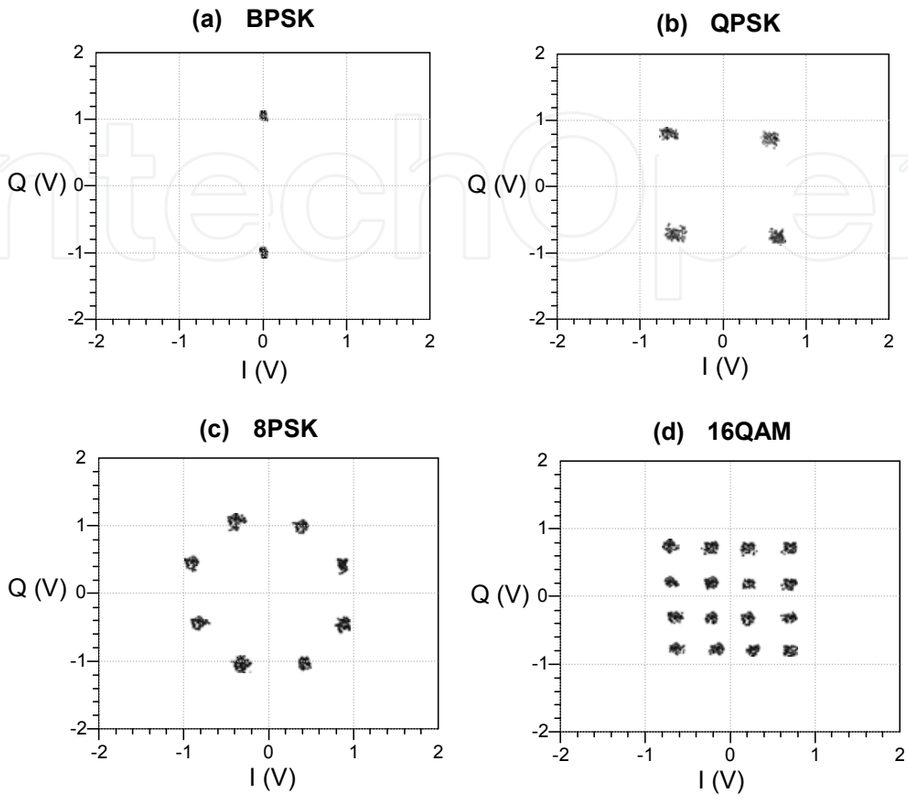

Fig. 28. Measurement results of various PSK/QAM modulated signals using a Ka-band multi-port demodulator

In addition, Fig. 29 (b) shows simulated and measured results on QPSK signals BER vs. the phase shift from synchronism between the carrier and LO signals, when both frequencies are set at 27 GHz. The simulated and measured BER is less than 1.0 E^{-6} for LO phase shift from the synchronism smaller than ± 35° and ± 30°, respectively.

Fig. 30 shows the schematic block diagram of a 60 GHz wireless link using a multi-port module (MPM) (Moldovan et al., 2008). The receiver uses a multi-port heterodyne architecture with rapid analog carrier recovery loop at IF. Two IF differential amplifiers (IFDA) will generate quadrature IF signals. A second down-conversion, IF to baseband, is performed using two conventional mixers and the carrier recovery module (CRM). This CRM generates the IF coherent signal of 900 MHz.

A rapid analog carrier recovery loop was chosen for synchronous demodulation, in order to follow the inherent frequency/phase shift of the millimeter-wave frequency local oscillator (LO) and the eventual Doppler shift due to relative movements between transmitter and receiver. After low pass filtering (LPF) and baseband amplification (BBA), the quadrature baseband demodulated signals are obtained at the outputs of the sample and hold circuits (SHC). A clock recovery circuit generates an

in-phase clock at the symbol rate using one of the outputs. The use of two limiters improves the demodulated QPSK signals at the baseband module (BBM) output.

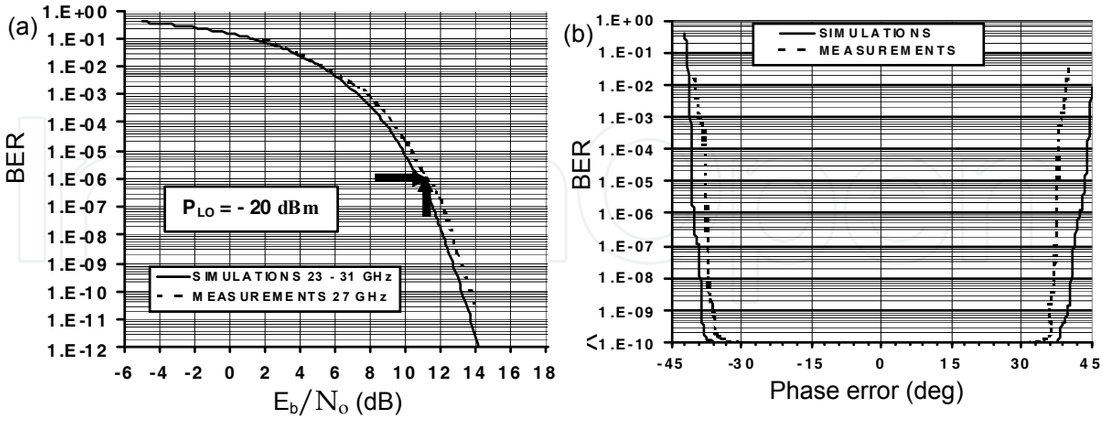

Fig. 29. BER results of QPSK modulated signals versus E_b/N_o ratio (a) and phase error from synchronism (b)

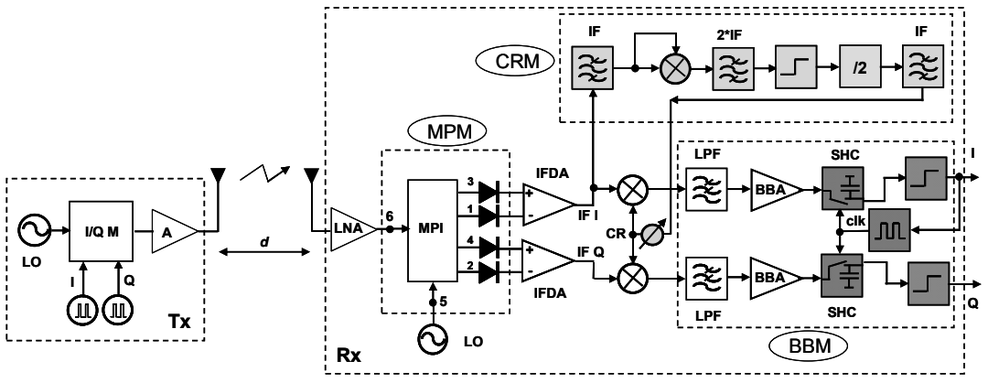

Fig. 30. Schematic block diagram of 60 GHz wireless link using a multi-port heterodyne architecture with carrier recovery loop at IF

Simulations are performed using a 60 GHz carrier frequency and a pseudorandom signal, which drives the direct millimeter-wave QPSK modulator. The bit-rate is chosen at 500 Mb/s with a corresponding symbol rate of 250 MHz. The transmitter power is set at 10 dBm, and the antenna gains are 10 dBi. A loss-link model based on the Friis equation is used to simulate the signal propagation over the distance d of 10 m. In order to obtain realistic results, the multi-port model is based on measurement results of the V-band circuit (see Figs. 11 and 12).

Bit error rate analysis is also performed using an appropriate length pseudorandom bit stream and various Doppler shifts. Fig. 31 shows the BER results versus the energy per bit to the spectral noise density (E_b/N_o), in the case of an ideal QPSK demodulator, a Doppler shift up to 200 KHz, and a Doppler shift of 600 KHz. The simulation results show a very good performance of the proposed wireless link: the BER is 10^{-6} for an E_b/N_o ratio of 10.4 dB,

similar to the ideal demodulator, if the Doppler shift is less than 200 KHz (circles on the BER diagram). For a Doppler shift of 600 KHz, corresponding to a millimeter-wave LO frequency stability of 10^{-5}, the BER is less than 10^{-6} for an E_b/N_o ratio of around 13.5 dB. Therefore, the E_b/N_o ratio of the received 600 KHz Doppler shift signal must increase with 3 dB for similar results, as in the ideal case. The BER value deteriorates from 10^{-6} to around 10^{-3} for a E_b/N_o ratio of 10.4, remaining at a reasonable level. Transmission on range up to 10 m, as required for UWB short range WPAN, has been demonstrated using previous simulations based on S-parameters measurement results of a ceramic V-band multi-port. A multi-port receiver prototype based on previous results is currently under design.

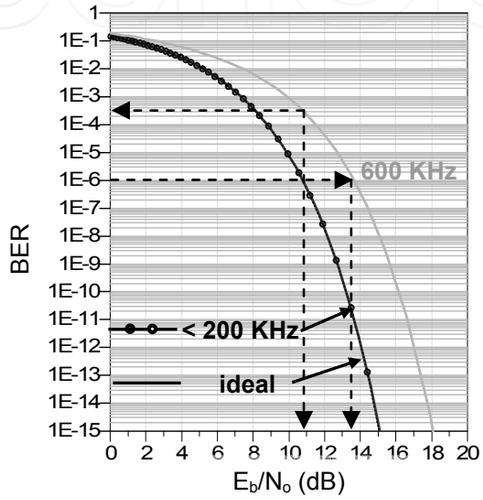

Fig. 31. BER simulation results for various Doppler shifts

4.2 Radar Sensor Applications

4.2.1 Two-tone CW W-band Multi-port Radar

This method uses two CW signals to measure both relative speed and distance to the target (Moldovan et al, 2007).

The relative speed of the target is obtained by measuring one of the I or Q signal frequency, according to the equation:

$$v = \frac{c}{2} \cdot \frac{\omega - \omega_0}{\omega_0} \tag{46}$$

where c is the speed of light, and ω and ω_0 are the transmitted and reflected signal frequencies, respectively.

The direction of target movement is obtained by a simple observation; the sense of rotation of $\Gamma = I + jQ$ phasor in the complex plane, clockwise or counter clockwise, is related to the sign of the Doppler frequency.

The distance measurement is obtained using two adequately spaced CW frequencies ω_{01} and ω_{02}. The distance to the target is calculated using the measured difference between the phases of the two corresponding echo signals $\Delta\theta_1$ and $\Delta\theta_2$ respectively:

$$d = \frac{c}{2} \cdot \frac{\Delta\theta_1 - \Delta\theta_2}{\omega_{01} - \omega_{02}} \tag{47}$$

A radar sensor prototype (see Fig. 32) operating at 94 GHz was built using the SIW circuit in brass fixture of Fig. 21, external components as wave-guide antennas, attenuator (Att), phase shifter (PhSh) and a baseband module to generate I/Q signals according to multi-port theory (Moldovan et al., 2007). The metallic target is placed in the vicinity of the sensor. Therefore the CW signal frequencies are spaced by 50 MHz, corresponding to a maximum unambiguous range of 3 m. A distance measurement error of 2% is obtained validating the operating principle of this radar sensor.

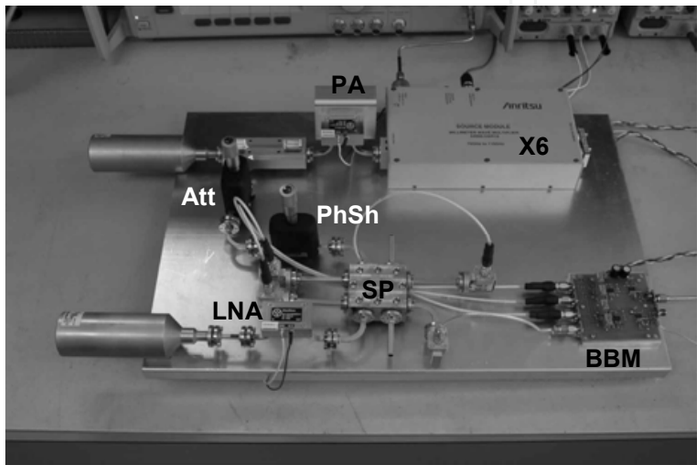

Fig. 32. Two-tone W-band multi-port radar sensor prototype

4.2.2 FMCW and PCCW V-band Multi-port Radar

Frequency modulated (FM) and phase coded (PC) CW radar sensor architectures are explored in conjunction with the V-band multi-ports presented in Fig. 15 (Cojocaru et al., 2008, 2009).

The FMCW radars transmit linear modulated continuous wave signals, which are positive and negative modulated, alternatively. The frequency difference of the transmitted and received signals is used to obtain relative speed and the distance to the target.

It is to be noted that phase coded (PC) waveforms comparative to FM waveforms differ in the sense that the transmitted pulse is subdivided into a number of equal length sub-pulses. The phase of each sub-pulse is chosen according to an optimal binary code sequence. An optimal binary code consists of a sequence of +1s and -1s (i.e. the phase alternates between 0° and 180°), and it has some remarkable features. Firstly, the peak side lobe of the autocorrelation function is the minimum possible for a given sequence length and secondly, the compression ratio is equal to the number of elements of the code. Thus, upon reception, the compressed pulse obtained through the correlation will enable the range to target evaluation.

In order to obtain initial validation of the proposed architectures, system simulations are performed using multi-port computer models based on S-parameter measurements in an ADS co-simulation platform. These results show relative speed and range measurements

with a good accuracy. The principle of the Doppler shift sign detection, related to multi-port proprieties is demonstrated. The proposed PCCW architecture effectively rejects the Doppler frequency from the range channel, before the correlation takes place, providing an accurate pulse compression.
Two prototype front-ends are currently under design and fabrication.

5. Conclusion

The chapter illustrates the interferometric concept in quadrature down-conversion for communication and radar sensor applications. Various millimeter-wave multi-port circuits covering the Ka, V and W bands are presented and analyzed. In addition, a Ka band demodulator and a W-band radar sensor prototype are presented. Present and future works are focused on UWB multi-port receivers and V-band radar sensors for automotive applications.
The multi-port circuits can successfully replace conventional quadrature mixers and the proposed architectures exploit the advantages of millimeter-wave interferometry, as presented in this chapter.

6. References

Boukari, B., Hammou, D., Moldovan, E., Bosisio, R., Wu, K. & Tatu, S.O. (2009). MHMICs on Ceramic Substrate for Advanced Millimeter wave Systems, *Proceedings of IEEE Microwave Theory and Techniques Symposium*, pp. 1025-1028, Boston, June 7-12, 2009.

Cojocaru, R.I., Moldovan, E., Boukari, B., Affes, S. & Tatu, S.O. (2008). A New 77 GHz Automotive Phase Coded CW Multi-port Radar Sensor Architecture. *Proceedings of 5th European Radar Conference European Microwave Week*, pp. 164-167, Amsterdam, October 27-31, 2008.

Cojocaru, R.I., Boukari, B., Moldovan, E. & Tatu, S.O. (2009). Improved FMCW Multi-Port Technique, *Proceedings of 6th European Radar Conference 2009 European Microwave Week*, Rome, September 28 – October 2, 2009, pp. 290-293.

Cohn, S.B. & Weinhouse, N.P. (1964). An Automatic Microwave Phase Measurement System. *Microwave Journal*, Vol. 7, pp. 49-56, February 1964.

Engen, G.F. & Hoer, C.A. (1972). Application of an Arbitrary 6-Port Junction to Power-Measurement Problems. *IEEE Transactions on Instrumentation and Measurement*, Vol. 21, No. 11, pp. 470-474, November 1972.

Engen, G.F. (1977). a. The Six-Port Reflectometer. An Alternative Network Analyzer. *IEEE Transactions on Microwave Theory and Techniques*, Vol. 25, No. 12, pp. 1075-1077, December 1977.

Engen, G.F. (1977). b. An Improved Circuit for Implementing the Six-Port Technique of Microwave Measurements. *IEEE Transactions on Microwave Theory and Techniques*, Vol. 25, No. 12, pp. 1080-1083, December 1977.

Li, J., Wu, Ke & Bosisio, R.G. (1994). A Collision Avoidance Radar Using Six-Port Phase/Frequency Discriminator (SPFD). *Proceedings of IEEE Microwave Theory and Techniques Symposium*, pp. 1553-1556, 1994.

Li, J., Bosisio, R.G. & Wu, K. (1995). Computer and Measurement Simulation of a New Digital Receiver Operating Directly at Millimeter-Wave Frequencies. *IEEE Transactions Microwave Theory Techniques*, Vol. 43, pp. 2766-2772, December 1995.

Li, J., Bosisio, R.G. & Wu, K. (1996). Dual-Ton Calibration of Six-Port Junction and Its Application to the Six-Port Direct Digital Millimetric Receiver. *IEEE Transactions Microwave Theory Techniques*, Vol. 44, pp. 93-99, January 1996.

Moldovan, E., Tatu, S.O., Gaman, T., Wu, Ke & Bosisio, R.G. (2004). A New 94-GHz Six-Port Collision-Avoidance Radar Sensor. *IEEE Transactions on Microwave Theory and Techniques*, Vol. 52, No. 3, pp. 751-759, March 2004.

Moldovan, E., Bosisio, R.G. & Wu, Ke (2006). W-Band Multiport Substrate-Integrated Waveguide Circuits. *IEEE Transactions on Microwave Theory and Techniques*, Vol. 54, No. 2, pp. 625-632, February 2006.

Moldovan, E., Tatu, S.O., Affes, S, Wu, K. & Bosisio, R. (2007). W-band Substrate Integrated Waveguide Radar Sensor Based on Multi-port Technology, *Proceedings of 4th European Radar Conference*, *European Microwave Week*, pp. 174-177, Munich, October 8 - 12, 2007.

Moldovan, E., Affes, S. & Tatu, S.O. (2008). A 60 GHz Multi-Port Receiver with Analog Carrier Recovery for Ultra Wideband Wireless Personal Area Networks, *Proceedings of European Microwave Conference*, *European Microwave Week*, pp. 1779-1782, Amsterdam, October 27-31, 2008.

Tatu, S.O., Moldovan, E., Wu, Ke & Bosisio, R.G. (2001). A New Direct Millimeter Wave Six-Port Receiver. *IEEE Transactions on Microwave Theory and Techniques*, Vol. 49, No. 12, pp. 2517-2522, December 2001.

Tatu, S.O., Moldovan, E., Brehm, G., Wu, Ke & Bosisio, R.G. (2002). Ka-Band Direct Digital Receiver. *IEEE Transactions on Microwave Theory and Techniques*, Vol. 50, No. 11, pp. 2436-2442, November 2002.

Tatu, S.O., Moldovan, E., Wu, Ke, Bosisio, R.G. & Denidni, T. (2005). Ka-Band Analog Front-End for Software - Defined Direct Conversion Receiver. *IEEE Transactions on Microwave Theory and Techniques*, Vol. 53, No. 9, pp. 2768-2776, September 2005.

Tatu, S.O. & Moldovan, E. (2007). V-Band Multiport Heterodyne Receiver for High-Speed Communication Systems. *EURASIP Journal on Wireless Communications and Networking*, Vol. 2007, Article ID 34358, 7 pages, Hindawi Publishing Corp., 2007

Microwave and Millimeter Wave Technologies Modern UWB antennas and equipment
Edited by Igor Mini

ISBN 978-953-7619-67-1
Hard cover, 488 pages
Publisher InTech
Published online 01, March, 2010
Published in print edition March, 2010

How to reference
In order to correctly reference this scholarly work, feel free to copy and paste the following:

Moldovan Emilia, Bosisio G. Renato, Wu Ke and Tatu Serioja O. (2010). Multi-Port Technology and Applications, Microwave and Millimeter Wave Technologies Modern UWB antennas and equipment, Igor Mini (Ed.), ISBN: 978-953-7619-67-1, InTech, Available from: http://www.intechopen.com/books/microwave-and-millimeter-wave-technologies-modern-uwb-antennas-and-equipment/multi-port-technology-and-applications

INTECH
open science | open minds

InTech Europe
University Campus STeP Ri
Slavka Krautzeka 83/A
51000 Rijeka, Croatia
Phone: +385 (51) 770 447
Fax: +385 (51) 686 166
www.intechopen.com

InTech China
Unit 405, Office Block, Hotel Equatorial Shanghai
No.65, Yan An Road (West), Shanghai, 200040, China
中国上海市延安西路65号上海国际贵都大饭店办公楼405单元
Phone: +86-21-62489820
Fax: +86-21-62489821

IntechOpen